coatings

MDPI

Article

Relevant Aspects of Piranha Passivation in Ti6Al4V Alloy Dental Meshes

Nuno Cruz [1], Javier Gil [1,2,*], Miquel Punset [3,4,5,6], José María Manero [3,4,6], João Paulo Tondela [7,*], Pablo Verdeguer [1], Conrado Aparicio [2] and Elisa Rúperez [3,4,6]

1 Bioengineering Institute of Technology, International University of Catalonia (UIC), 08195 Barcelona, Spain; nuno.cruz@orismed.pt (N.C.); pabloverdeguerm@gmail.com (P.V.)
2 School of Dentistry, International University of Catalonia (UIC), 08195 Barcelona, Spain; cjaparicio@uic.es
3 Biomaterials, Biomechanics and Tissue Engineering Group (BBT), Department of Materials Science and Engineering, Technical University of Catalonia (UPC), 08019 Barcelona, Spain; miquel.punset@upc.edu (M.P.); jose.maria.manero@upc.edu (J.M.M.); elisa.ruperez@upc.edu (E.R.)
4 Barcelona Research Centre in Multiscale Science and Engineering, Technical University of Catalonia (UPC), 08019 Barcelona, Spain
5 Innovation and Technology Center (CIT), Polytechnic University of Catalonia (UPC), 08034 Barcelona, Spain
6 Sant Joan de Déu Research Institute (IRSJD), 08034 Barcelona, Spain
7 CIROS from the Faculty of Medicine, University of Coimbra, FMUC, 3004-531 Coimbra, Portugal
* Correspondence: xavier.gil@uic.es (J.G.); jtondela@fmed.uc.pt (J.P.T.)

Abstract: Passivation of titanium alloy dental meshes cleans their surface and forms a thin layer of protective oxide (TiO_2) on the surface of the material to improve resistance to corrosion and prevent release of ions to the physiological environment. The most common chemical agent for the passivation process of titanium meshes is hydrochloric acid (HCl). In this work, we introduce the use of Piranha solution (H_2SO_4 and H_2O_2) as a passivating and bactericidal agent for metallic dental meshes. Meshes of grade 5 titanium alloy (Ti6Al4V) were tested after different treatments: as-received control (Ctr), passivated by HCl, and passivated by Piranha solution. Physical-chemical characterization of all treated surfaces was carried out by scanning electron microscopy (SEM), confocal microscopy and sessile drop goniometry to assess meshes' topography, elemental composition, roughness, wettability and surface free energy, that is, relevant properties with potential effects for the biological response of the material. Moreover, open circuit potential and potentiodynamic tests were carried out to evaluate the corrosion behavior of the differently-treated meshes under physiological conditions. Ion release tests were conducted using Inductively Coupled Plasma mass spectrometry (ICP-MS). The antibacterial activity by prevention of bacterial adhesion tests on the meshes was performed for two different bacterial strains, *Pseudomonas aeruginosa* (Gram-) and *Streptococcus sanguinis* (Gram+). Additionally, a bacterial viability study was performed with the LIVE/DEAD test. We complemented the antibacterial study by counting cells attached to the surface of the meshes visualized by SEM. Our results showed that the passivation of titanium meshes with Piranha solution improved their hydrophilicity and conferred a notably higher bactericidal activity in comparison with the meshes passivated with HCl. This unique response can be attributed to differences in the obtained nanotextures of the TiO_2 layer. However, Piranha solution treatment decreased electrochemical stability and increased ion release as a result of the porous coating formed on the treated surfaces, which can compromise their corrosion resistance. Framed by the limitations of this work, we conclude that using Piranha solution is a viable alternative method for passivating titanium dental meshes with beneficial antibacterial properties that merits further validation for its translation as a treatment applied to clinically-used meshes.

Keywords: titanium; dental meshes; passivation; piranha; corrosion resistance; ion release; bacterial adhesion

Citation: Cruz, N.; Gil, J.; Punset, M.; Manero, J.M.; Tondela, J.P.; Verdeguer, P.; Aparicio, C.; Rúperez, E. Relevant Aspects of Piranha Passivation in Ti6Al4V Alloy Dental Meshes. *Coatings* **2022**, *12*, 154. https://doi.org/10.3390/coatings12020154

Academic Editors: Jasmina Primožič and Vincenzo D'Antò

Received: 28 December 2021
Accepted: 24 January 2022
Published: 27 January 2022

1. Introduction

The amount of bone is paramount to predictably achieve success and long-term survival of implant-supported rehabilitations. Actually, implant dentistry has evolved to a prosthetically driven implant placement concept, meaning that biology, biomechanics, function and esthetics of the implant supported rehabilitation should be considered for the adequate implant position in bone. Although proper amount of bone is needed to go along with the esthetical and functional prosthetic design, variable discrepancies in the available bone are seldom found. This may occur because of prolonged tooth loss, trauma, injury or bone disease and resection, conducting to a horizontal, vertical or combined bone defect (Siebert). Hence, several techniques and materials for bone augmentation have been used concomitant with implant placement or as a staged approach [1–4].

Following the biological principles of selective cell exclusion for regenerative wound healing and guided tissue regeneration, these were later proven to be applicable to guided bone regeneration also. Techniques involve placing a mechanical barrier to protect the blood clot and to isolate the bony defect from the surrounding connective and epithelial tissue invasion. This space is needed to allow the osteoblasts to access the space intended for bone regeneration [5,6].

Titanium rigid scaffolds were successfully used for bone augmentation, even outside of the bone envelope. Presently, one mainstream direction for 3D printing is biomedical applications, specifically in creating scaffolds for medical implants such as individualized titanium meshes for bone regeneration [7–9]. In recent years, the development of personalized rapid prototyping medical devices based on the digital imaging and communications in medicine (DICOM) files provided by computerized tomography/cone beam computerized tomography (CT/CBCT) scans has deeply intensified [10]. Based on the patient's bone defect and resorting to computer aided design (CAD) software, it is possible to design medical devices with the intent of recreating the lost tridimensional bone anatomy.

Regardless of the production technique for any implantable devices, it is mandatory to control the characteristics such as permeability, surface topography and roughness, and optimize their biological performance [11–16]. High degrees of roughness represent a major risk for ionic leakage from the material [17] and the bacterial adhesion can be increased, with the consequence of implant failures [10]. Smooth surfaces are able to slow down the biological processes at the interface, keeping the titanium oxidized layer properties unaffected for longer time periods [9]. The associated correct micro- and nano-roughness level can stimulate osteoblast differentiation, proliferation and production of both matrix and local growth factors [10]. Furthermore, changes in roughness correlate with selective protein adsorption, collagen synthesis and the maturation of chondrocytes, which all significantly influence the implant's osseointegration [10].

It is well known that the implant–living tissues interactions depend on the surface properties, such as roughness, wettability, surface energy and chemical composition, among others. Biomaterials research should optimize, at different scales, the surface characteristics in order to improve different functions: bioactivity, osseointegration or bactericide behavior. In addition, titanium meshes are susceptible to corrosion due to the presence of metals of different chemical nature in the mouth, as well as the release of titanium ions into the environment which must be taken into account [11–13]. It has been long recognized that the corrosion products formed as a result of metal–environment interactions have a significant bearing on the biocompatibility and long-term stability of the prostheses/implant. The material used must not cause any biological adverse reaction and must retain its form and properties [11,12] during function. Human stomatognathus is subjected to varying changes in pH and temperature owing to differences in local, systemic, environmental, economic and social conditions for each individual. Corrosion can result from the presence of a number of corrosive species such as hydrogen ion (H^+), sulfide compounds (S^{2-}), dissolved oxygen, free radicals (O^{2-}, O^-), and chloride ion (Cl^-) resulting in the metal surface breakdown and a consequent adverse tissue reaction [13]. In addition, the effect of

bacteria can lead to the appearance of bacterial plaque which will affect bone regeneration and cause inflammation in the patient [14–16].

Passivation is, in general, an oxidation reaction obtained by chemical or electrochemical process which promotes the formation and increasing of the thickness of protective layers [10–13]. The effect of passivation and oxidative agents and the role of titanium oxide as the physico-chemical characteristics of the surface are poorly studied and understood [17–20].

In vitro studies have implied that the negatively charged and hydrophilic TiO_2 layer is, in fact, the key factor for the overall biocompatibility as it regulates the protein adsorption [9]. For the particular case of the dentistry, countless studies have already been conducted in order to guarantee the implantation safety. Usually, no inflammatory response signs are found in the oral tissue adjacent to titanium implants; however, it is important to note that for some patients, hypersensitivity can be induced [9].

In this work, the aim was to study an alternative passivation method using the so-called Piranha solution. The Piranha solution is a mixture of sulfuric acid and hydrogen peroxide. We studied the effects of Piranha solution treatment on surface physical-chemical properties, chemical degradation (corrosion and release of ions) and antimicrobial activity against Gram-positive and Gram-negative bacteria.

2. Materials and Methods

2.1. Samples

One hundred twenty Grade 5 titanium alloy (Ti6Al4V) meshes (BoneEasy, Arada, Portugal) were used. Figure 1 shows the mesh and its application as a membrane with calcium phosphate.

We worked with 3 groups of samples:

Control: as-received material.

HCl passivation: The meshes were immersed in a solution of hydrochloric acid (HCl) 20% (v) for 40 s at room temperature (HCl group). This is the gold-standard passivation treatment for dental implants and prosthesis.

Piranha passivation: The meshes were immersed in a solution of Piranha, which is a mixture of sulfuric acid 96% (v) and a 50:50 ratio of hydrochloric acid (HCl) 20% (v) and hydrogen peroxide 30% (v) for 2 h.

Piranha solutions are a mixture of concentrated sulfuric acid with hydrogen peroxide, usually in a ratio of 3:1 to 7:1. They are used to remove trace amounts of organic residues, such as photoresist, from substrates. The mixing procedure is an exothermic reaction that can reach temperatures of 100 °C or higher. The reaction of hydrogen peroxide on concentrated sulfuric acid produces highly activated and oxidizing peroxymonosulfuric acid (H_2SO_5), also called Caro's acid [1]. However, there are many different mixture ratios that are commonly used, and all are called Piranha. The addition of NH_4OH in order to accelerate the decomposition of H_2O_2 or the addition of HCl, as in this research, favors cleanness and increases the oxide stabilization. Piranha solution must be prepared with great care. It is highly corrosive and an extremely powerful oxidizer. Surfaces must be reasonably clean and completely free of organic solvents from previous washing steps before coming into contact with the solution. Piranha solution cleans by decomposing organic contaminants, and a large amount of contaminant will cause violent bubbling and a release of gas that can cause an explosion [21].

After treatment, all samples were cleaned a sequence of 3 ultrasonic baths (3 min each): two consecutive with distilled water, followed by one with ethanol.

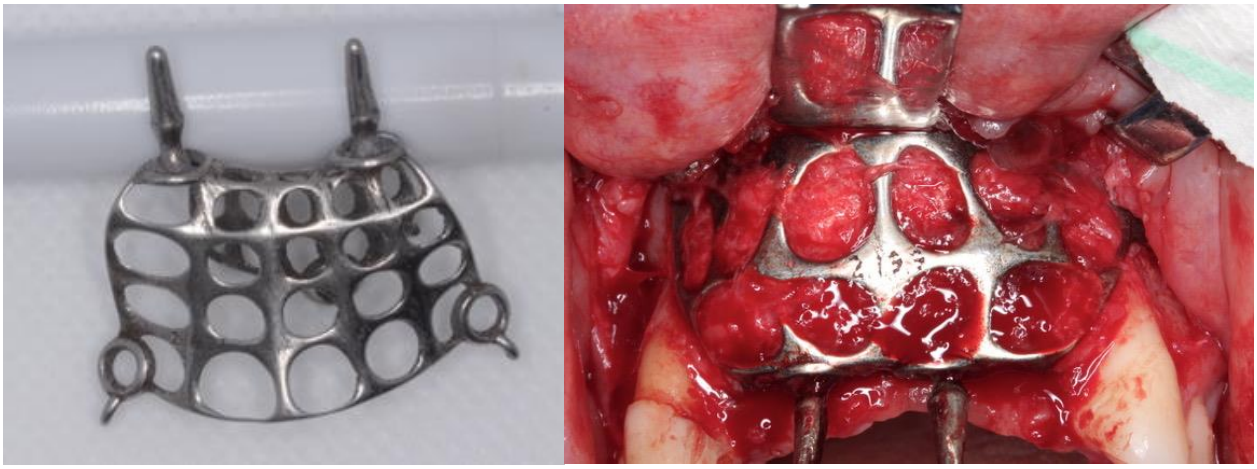

Figure 1. Grade 5 titanium mesh used in this study.

2.2. Surface Characterization

Roughness for all groups was determined using an Olympus LEXT OLS3100 confocal microscope (Olympus, Tokyo, Japan). Three samples per group were tested and 3 measurements per sample were taken at ×1000 magnification. The parameters Ra and Rz were determined. Ra corresponds to the arithmetic mean of the absolute values of the deviations of the profiles of a given length of the sample. Rz corresponds to the sum of the maximum peak height and the maximum valley depth within the sampling length [21].

The water sessile drop technique was used for the measurement of the contact angle, θ, formed between the water drop and the surface. The greater the contact angle, the lower the wettability and vice versa. For angles less than 10°, the surface is considered superhydrophilic, for angles between 10° and 90° surfaces are hydrophilic and for angles greater than 90°, surfaces are considered hydrophobic. A droplet generation system equipped with a 500 µL Hamilton syringe with micrometric displacement control was used to control the volume (3 µL) and to deposit the droplet. The analysis was performed using a gonyometer with drop profile image capture (Contact Angle System OCA15plus, DataPhysics, Filderstadt, Germany) and analyzed with SCA20 software (DataPhysics, Filderstadt, Germany) [22,23].

To calculate the surface free energy, the contact angle was measured with two different liquids, water and diiodomethane. The contact angle measurements of diiodomethane were obtained following the same procedure used to measure water contact angles [22]. The surface free energy and its polar (γ^p) and dispersive (γ^d) components were then calculated using the Owens and Wendt equation [17]:

$$\gamma_L \cdot (1 + \cos\theta) = 2 \cdot ((\gamma_L^d \cdot \gamma_S^d)^{1/2} + (\gamma_L^p \cdot \gamma_S^p)^{1/2}) \quad (1)$$

Surface morphology of the samples was analyzed with a focused ion beam Zeiss Neon40 FE-SEM (Carl Zeiss NTS GmbH, Oberkochen, Germany). Images of uncoated samples were taken at a working distance of 7 mm and an accelerating voltage of 5 kV. An EDS detector (INCA PentaFETx3 system, Oxford Instruments, Abingdon, UK) was used to detect silver presence on the surface of the samples. This microscope has a resolving power of 3 nm and allows the observation of the nanotextures produced by the reaction of the Piranha solution with the Ti6Al4V alloy.

2.3. Corrosion Behavior

A total of 60 samples, (n = 20) for each group of samples, were used for the corrosion tests. The test area for each sample was 19.6 mm^2. The electrolyte for all tests was Hank's solution (Table 1), which is a saline fluid that closely captures the ion composition of the human serum environment.

Table 1. Composition of Hank's solution.

Chemical Product	Composition (mM)
K_2HPO_4	0.44
KCl	5.4
$CaCl_2$	1.3
Na_2HPO_4	0.25
NaCl	137
$NaHCO_3$	4.2
$MgSO_4$	1.0
$C_6H_{12}O_6$	5.5

The electrochemical cell used was a polypropylene (PP) container with a capacity of 185 mL and a methacrylate lid with 6 holes for the introduction of the sample, the reference electrode and the counter electrode (Figure 2). For both the open circuit potential measurement tests and the potentiodynamic tests, the reference electrode used was a calomel electrode (saturated KCl), with a potential of 0.241 V compared to the standard hydrogen electrode. All tests were performed at room temperature and in a Faraday cage to avoid the interaction of external electric fields.

For the open circuit potential measurement tests, only the sample and the reference electrode were placed in the electrochemical cell. Tests were carried out for 5 h for all the samples, taking measurements every 10 s. The potential was considered to be stabilized when the variation of the potential is less than 2 mV over a period of 30 min as indicated in the ASTM G31 standard [23]. This test assesses which materials are more noble (higher potential) and thus, less susceptible to corrode. The data and the E-t curves were obtained using the PowerSuite software (Schneieder Electric, Ruil-Malmaison, France) with the PowerCorr-Open circuit (Schneieder Electric, Ruil-Malmaison, France).

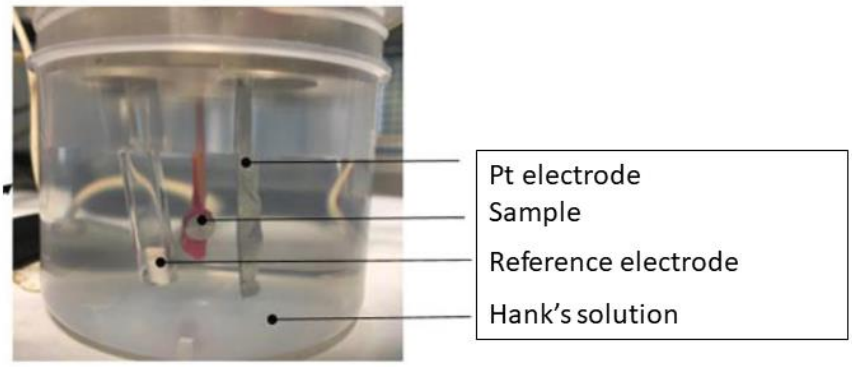

Figure 2. Experimental set up used for assessing corrosion resistance.

Cyclic potentiodynamic polarization curves were obtained for the 3 study groups following the ASTM G5 standard. In this test, a variable electrical potential is imposed by the potentiostat between the sample and the reference electrode, causing a current to flow between the sample and the counter electrode. The counter electrode used was platinum [17,24,25]. Before starting the test, the system was allowed to stabilize by means of an open circuit test for 1 h. After stabilization, the potentiodynamic test was launched, performing a cyclic sweep from −0.8 mV to 1.7 mV at a speed of 2 mV/s. These parameters were entered into the PowerSuite program using the PowerCorr-Cyclic Polarization function to obtain the curves. The parameters studied were:

1. i_{corr} ($\mu A/cm^2$)—corrosion current density;
2. E_{corr} (mV)—corrosion potential: value at which the current density changes from cathodic to anodic;
3. E_{rep} (mV)—repassivation potential: potential at which the passive layer regenerates;
4. E_p (mV)—pitting potential: value at which pitting corrosion may occur;

5. i_p (μA/cm^2)—passivation current density;
6. ip (μA/cm^2)—repassivation current density.

The E_{corr} and i_{corr} parameters are obtained by extrapolating the Taffel slopes. The Taffel slopes are also used to obtain the Taffel coefficients: anodic (βa) and cathodic (βc). These coefficients represent the slopes of the anodic and cathodic branch, respectively. In accordance with the ASTM G102-89 standard [23–26], these values are then used to calculate the polarization resistance (R_p) using the Stern–Geary expression and the corrosion rate (CR in mm/year) [24–28].

$$Rp = \frac{\beta a \cdot \beta c}{2.303 \cdot (\beta a + \beta c) \cdot i_{corr}} \quad (2)$$

The polarization resistance indicates the resistance of the sample to corrosion when subjected to small variations in potential. A total of 30 potentiodynamic tests were carried out, obtaining at least 10 curves per group.

$$CR = K_1 \cdot \frac{i_{corr}}{\rho} \cdot EW \quad (3)$$

2.4. Ion Release

Five samples from each group were used for the metal ion recovery test. After weighing the samples (m = 0.206 g) and following the ISO 10993-12 standard [26], a weight adjustment was made at the rate of 1 mL of Hank's solution for each 0.2 g of sample, as indicated in the standard. The 5 samples of each group were placed in the same Eppendorf with 5 mL of Hank's solution and stored at 37 °C. Hank's solution should be extracted and stored in the refrigerator after 1, 3, 7, 14 and 21 days. After each extraction, 5 mL of fresh Hank's solution has been replenished into the Eppendorf containing the samples. All Eppendorf tubes should be cleaned with 2% Nitric Acid and dried before use.

After 21 days, the concentration of released titanium ions was measured, at the test times indicated above, by inductively coupled plasma mass spectrometry (ICP-MS) with the Agilent Technologies 7800 ICP-MS.

2.5. Bacteria Analysis

Two types of bacteria, *P. aeruginosa* (Colección española de cultivos tipo, CECT 110, Valencia, Spain) and *S. sanguinis (*Culture Collection University of Gothenburg, CCUG 15915, Gothenburg, Sweden), a Gram-negative and a Gram-positive strain, respectively, were used for the bacterial adhesion test. Three samples per group and bacterial strain were tested.

The culture media and material (PBS) were previously sterilized by autoclaving at 121 °C for 30 min. Prior to the adhesion test, the samples were also sterilized. For this purpose, three 5 min ethanol washes were carried out in sterile culture plates. After removing the ethanol, the samples were exposed to ultraviolet light for another 30 min [29,30].

The agar plates were cultured at 37 °C for 24 h. From this culture, the liquid inoculum was prepared by suspending the bacteria in 5 mL of BHI (Brain Heart Infusion) and incubated for 24 h at 37 °C. The medium was then diluted to an optical density of 0.1 at a wavelength of 600 nm (OD600 = 0.1). For bacterial adhesion, enough solution with a concentration equivalent to OD600 = 0.1 to cover the surfaces (500 μL/sample) was introduced into the well of the culture plate of each sample and incubated at 37 °C for 1 h.

After this time, the samples were rinsed with PBS for 5 min twice and the bacteria were fixed with a 2.5% glutaraldehyde solution in PBS (30 min in the refrigerator). The glutaraldehyde solution was then removed and the samples were rinsed with PBS 3 times for 5 min. For viability analysis by confocal microscopy, the LIVE/DEAD BacLight bacterial viability kit (Thermo Fisher, Madrid, Spain) was used [13,14]. A solution was prepared with 1.5 μL of propidium in 1 mL of PBS. Using a micropipette, a drop of this solution (approximately 50 μL/sample) was deposited on the study surface and after incubation at room temperature in the dark for 15 min, the samples were rinsed 3 times with PBS for

5 min. The surfaces were then observed under a confocal microscope. Three images per sample were taken at 630× magnification (×63 objective). Wavelengths of 488 and 561 nm were used to detect bacteria with non-compromised membranes (LIVE) and compromised membranes (DEAD), respectively.

Prior to the observation of the samples by scanning electron microscopy (SEM), the samples were dehydrated. For the dehydration process and the critical point drying, 10 min washes were carried out with ethanol solutions of gradual concentrations of 30%, 50%, 70%, 80%, 90%, 95% and 100%. They were then left to dry for 24 h at room temperature. Then, samples were coated with platinum for 5 s before observation under the microscope. Ten images of each sample were taken at 20,000× magnifications for bacterial quantification on each surface.

2.6. Statistical Analysis

All results were expressed as mean and standard deviation except for the bacterial adhesion test results which were expressed as median and standard error. The comparative T.TEST (with the Excel software) was carried out between the different groups at 95%, which means that for values of $p < 0.05$, there are significant differences.

3. Results

Figure 3 shows SEM images of the surfaces of the titanium alloy after passivation treatments. No significant variations between the control and HCl treatment were detected and both types of surfaces clearly showed machining marks. Machining marks in HCl-passivated surfaces were lighter than in as-machined surfaces, probably due to the effect of the higher concentration of the acid. However, on the surface of the samples subjected to the Piranha passivation treatment, the acid attack almost completely removed the machining marks and, notably, produced a homogenously-distributed and commonly-obtained surface nanotexture in the form of nanocavities (Figure 4) [15].

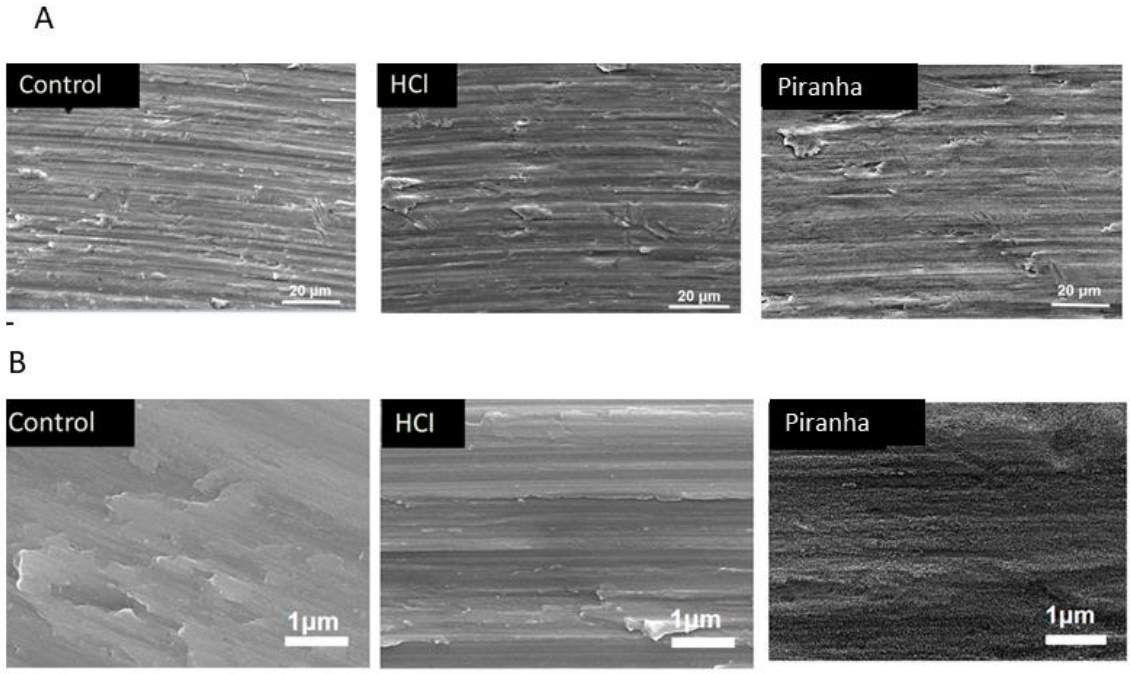

Figure 3. (**A**) Surfaces of grade 5 Ti alloy treated with different passivation methods; (**B**) at higher magnifications.

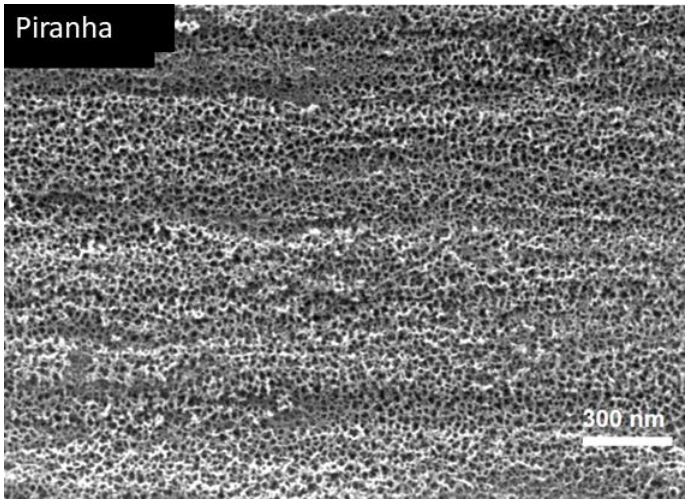

Figure 4. Nanotexture of titanium alloy after Piranha passivation treatment observed by high-resolution scanning electron microscopy.

The different passivation treatments on the titanium alloy meshes, either with HCl or Piranha solution, did not alter the average roughness (Ra), as no statistically significant differences were observed with respect to the control group (Table 2). However, the Piranha treatment showed statistically significant lower R_z values with respect to the other groups. These results suggest that the Piranha solution treatment attacked the titanium, reducing machining failures and creating an oxide layer that reduces the differences between valleys and peaks. The large difference between the R_a and R_z values shows that we have two types of texture (Figure 5), one associated with the turning marks responsible for the high R_z values and the other the nanotexture associated with the passivation treatment.

Table 2. Roughness values, R_a and R_z, for titanium alloy surfaces with different passivation treatments. Different letters in the same column denote statistically significant differences ($p < 0.05$) between groups.

Mesh	R_a (µm)	R_z (µm)
Control	0.12 ± 0.03 (a)	4.95 ± 0.76 (A)
HCl	0.14 ± 0.08 (a)	4.87 ± 0.90 (A)
Piranha	0.12 ± 0.05 (a)	1.90 ± 0.73 (B)

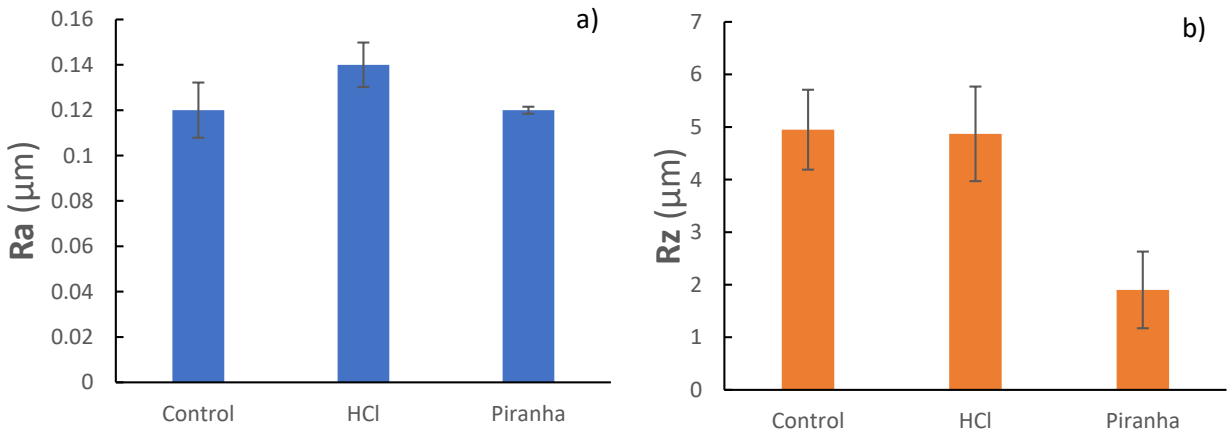

Figure 5. Roughness parameters quantified with different passivation conditions: (**a**) Ra and (**b**) Rz.

Wettability, i.e., hydrophilic/hydrophobic character of the tested surfaces, was determined measuring the water contact angle with the sessile drop technique (Table 3). Firstly, as-received control surfaces were hydrophobic with a contact angle higher than 90°. Secondly, all passivated surfaces had significantly higher hydrophilicity than untreated control surfaces. Thirdly, the surfaces passivated with Piranha solution produced a significantly higher hydrophilic material than the surfaces treated with HCl. Water contact angle, as well as polar and dispersive components of SFE, are plotted in Figure 6.

Corresponding with the results for the wettability of the different surfaces, the polar component of the surface free energy in the titanium alloy passivated with Piranha solution was the highest among all tested surfaces. The differences in the dispersive and polar components of the surface free energy for all tested surfaces were statistically significant [31–35].

It is widely accepted that increasing the polar component of a material's surface energy promotes initial adhesion and cell proliferation [17].

Table 3. Contact angles and components of the surface free energy for the differently passivated meshes.

Mesh	Θ Water (°)	Θ Diidomethane (°)	γ^d (mJ/m^2)	γ^p (mJ/m^2)	SFE (mJ/m^2)
Control	102.76 ± 7.00	48.40 ± 2.32	35.15 ± 1.28	0.12 ± 0.10	35.28 ± 1.35
HCl	86.37 ± 4.12	53.54 ± 0.92	32.39 ± 0.52	3.31 ± 1.28	35.70 ± 1.60
Piranha	49.05 ± 7.67	34.12 ± 3.94	42.37 ± 1.79	16.52 ± 4.22	58.90 ± 4.11

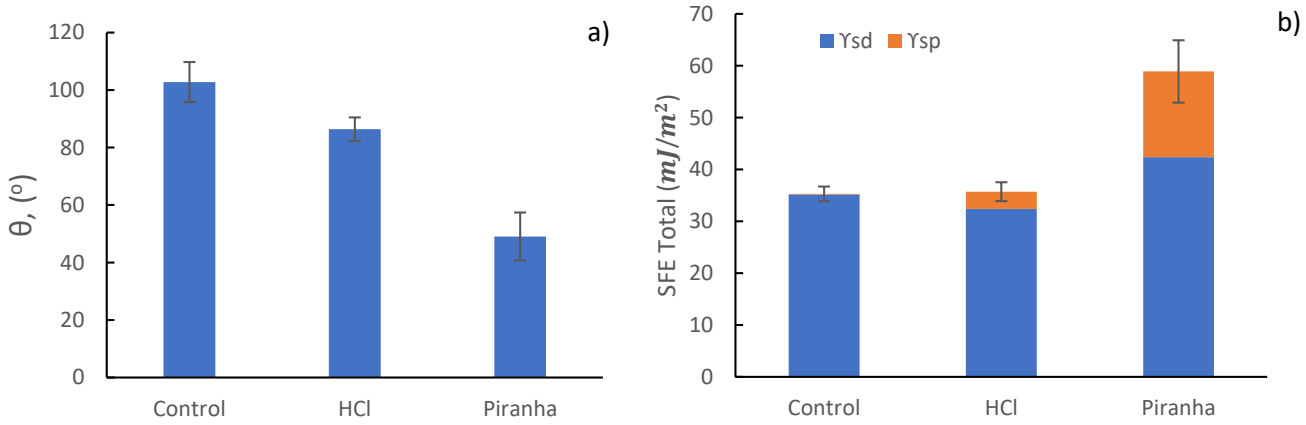

Figure 6. θ values (**a**) and SFE values (**b**) of cpTi treated with different passivation conditions.

Table 4 shows that the highest open circuit corrosion potential values (E_{OCP}) were obtained for titanium alloy surfaces treated with HCl. Therefore, HCl passivation produces the surfaces with the least tendency for corrosion, and therefore the best corrosion behavior. Conversely, surfaces treated with the Pirahna solution showed the lowest values in open circuit, which indicated the highest tendency for corrosion. The potentiodynamic studies confirmed that the treatment that produced surfaces with the best corrosion resistance was using HCl, as these passivated surfaces showed the lowest values of corrosion current density (i_{corr}) and corrosion rate (V_c). In addition, the HCl-treated samples show the highest resistance to polarization (R_p). The Piranha solution should produce the thickest protective TiO_2 layer; however, surfaces passivated with Piranha did not have an improved corrosion behavior with respect to the control samples. Moreover, only in samples treated with Piranha solution pitting corrosion could be observed after the potentiodynamic tests (Figure 7).

Table 4. Electrochemical and corrosion parameters assessed for Ti alloy meshes with different passivation treatments.

Mesh	E_{OCP} (mV)	i_{corr} (μA/cm^2)	R_p (MΩ/cm^2)	E_{corr} (V)	V_c (μm/Year)
Control	−196 ± 01	0.027 ± 0.008	2.428 ± 0.390	−361 ± 14	0.233 ± 0.066
HCl	−145 ± 11	0.018 ± 0.005	2.479 ± 0.083	−536 ± 39	0.176 ± 0.048
Piranha	−206 ± 27	0.056 ± 0.006	1.102 ± 0.149	−447 ± 26	0.488 ±0.047

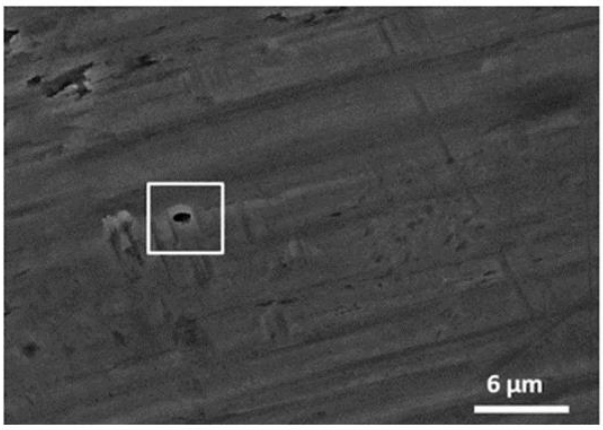

Figure 7. Pitting corrosion marks produced after completing the potentiodynamic test on a Grade 5 titanium alloy surface passivated with Piranha solution.

Table 5 shows the cumulative Ti ion release in parts per billion (ppb) from the passivated meshes in Hank's solution after increasing days of incubation, as can been observed in Figure 8. Analogous to the highest electrochemical stability, Ti ion release was the lowest from surfaces passivated with HCl, with a total cumulative concentration after 21 days of incubation of 4.1 ± 0.4 ppb, although with no statistically significant difference with respect to the untreated control group (7.0 ± 0.6 ppb). Differences are statistically significant when comparing Ti ion release from surfaces passivated with Pirahna solution and with HCl. Ion release from Piranha-treated titanium alloy meshes (10.3 ppb ± 0.9) more than doubled the ion release values from HCl-treated surfaces.

Table 5. Ti ion release (ppb) at different incubation times in Hank's solution.

Mesh	1 Day	3 Days	7 Days	14 Days	21 Days
Control	1.3 ± 0.2	2.7 ± 0.5	2.8 ± 0.3	4.5 ± 0.4	7.0 ± 0.6
HCl	1.0 ± 0.3	2.0 ± 0.2	2.1 ± 0.2	3.7 ± 0.3	4.1 ± 0.4
Piranha	2.2 ± 0.7	3.8 ± 0.2	4.2 ± 0.1	7.4 ± 0.9	10.3 ± 0.9

The higher ion release from surfaces treated with Piranha solutions with respect to the control and HCl-treated ones could be related to the higher corrosion rate and current density values, as previously presented. Corrosion phenomena are most likely the main cause of the degradation of the passive layer and the subsequent release of ions into the medium.

Quantitative analyses of the bacterial adhesion test performed with the Gram-negative *P. aeruginosa* and for the Gram-positive *S. sanguinis* show that there are no significant differences in the number of bacteria adhering to the surface of the control and HCl-treated surfaces, but there were significant differences with meshes treated with Piranha solution (Table 6). Indeed, for both bacterial strains, the Piranha-treated titanium alloy surfaces drastically reduced (at least one order of magnitude) bacterial adhesion in comparison to all

other groups (Figures 9 and 10). The bacteria adhered on the differently-treated surfaces can be observed in Figure 10 for *P. aeruginosa* and in Figure 11 for *S. sanguinis*, which supported the quantification differences assessed for bacterial adhesion. The LIVE/DEAD imaging revealed that differences in bacterial number were mainly related to prevention of bacteria colonization of the Piranha-treated surfaces as almost none of the bacteria remaining on the surfaces had their membranes compromised (red color).

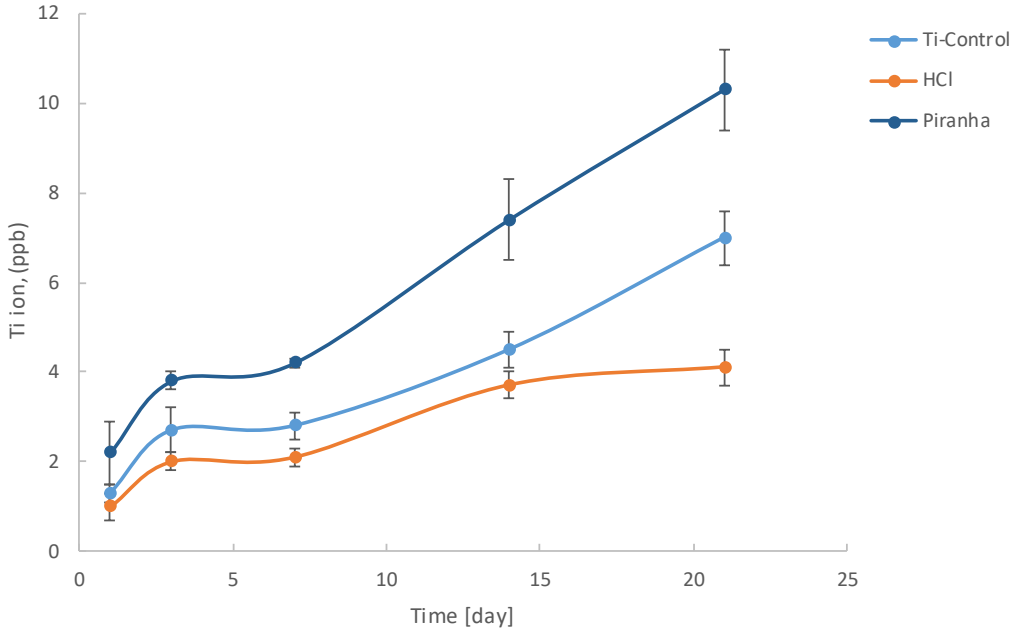

Figure 8. Ti ion release at different immersion times in Hank's solution of different passivation treatments on cpTi.

Table 6. Quantitative analysis of number of *P. aeruginosa* and *S. sanguinis* adhered on Grade 5 titanium alloy surfaces with different passivation treatments.

Mesh	*P. aeruginosa* (Number of Bacteria/mm^2)	*S. sanguinis* (Number of Bacteria/mm^2)
Control	$7.02 \times 10^5 \pm 0.52 \times 10^5$	$3.52 \times 10^5 \pm 0.48 \times 10^5$
HCl	$5.75 \times 10^5 \pm 0.33 \times 10^5$	$2.25 \times 10^5 \pm 0.13 \times 10^5$
Piranha	$1.23 \times 10^4 \pm 0.02 \times 10^4$	$5.03 \times 10^3 \pm 0.10 \times 10^3$

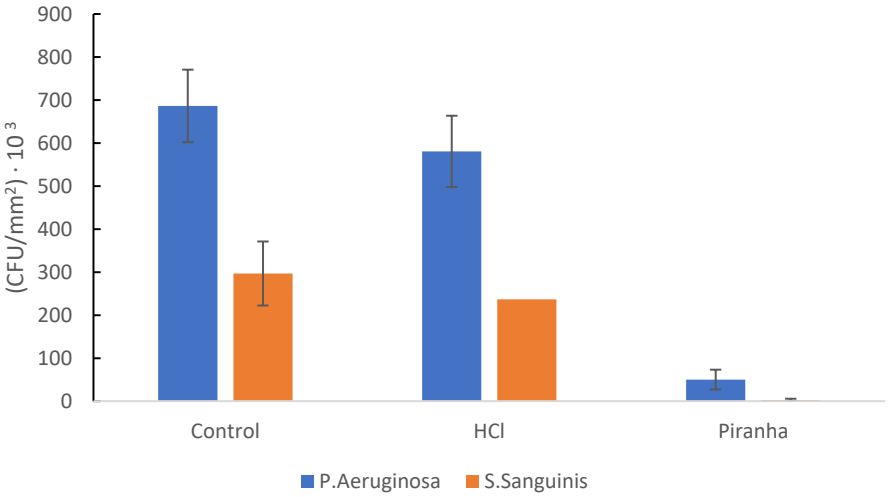

Figure 9. Analysis of *P. aeruginosa* and *S. sanguinis* adhesion for the three different conditions.

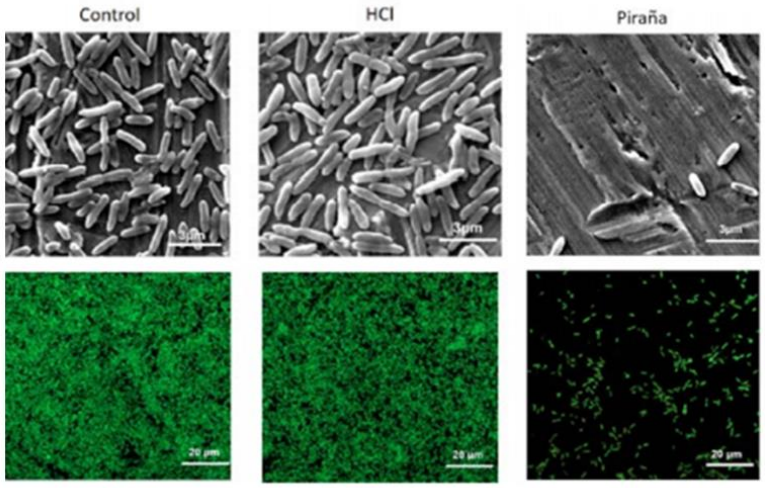

Figure 10. SEM (**top row**) and fluorescence (**bottom row**) images of *P. aeruginosa* stained by LIVE/DEAD.

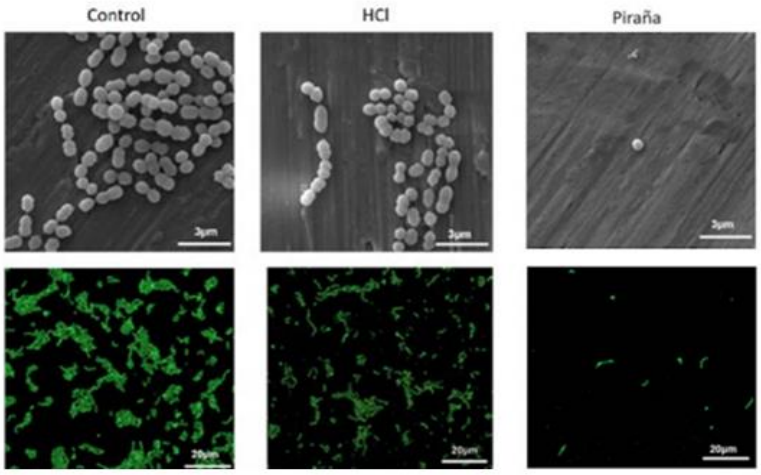

Figure 11. SEM (**top row**) and fluorescence (**bottom row**) images of *S. sanguinis* stained by LIVE/DEAD.

4. Discussion

The characteristic nanotexture [15,34–36] resulting from the passivation treatment of titanium alloy meshes with Pirahna solution (Figure 12) was a relevant surface property achieved with Piranha treatment in comparison to HCl treatment. Meshes treated with Piranha solution showed a submicrotexture with superimposed nanoporosity ranging from 9–20 nm. This surface topography was homogeneous and without cracks, which suggest a good toughness of the oxide layer formed. The presence of furrows on the treated surfaces might be related to a preferential etching process in areas with high internal energy, such as grain boundaries, dislocation pile-ups or other metallurgical or crystallographic singularities.

Notably, all passivation treatments tested increased hydrophilicity and surface free energy (Table 3). This suggests that passivating titanium meshes would not only produce a protective oxide layer but could also increase the meshes' interactions with the biological environment, favoring water, water-mediated and cellular–bacterial interactions. In most cases, protein adsorption and cell adhesion and proliferation have been correlated with an increase in surface hydrophilicity and the polar component of the surface free energy [36,37]. In particular, fibroblasts are sensitive to variations in wettability, and cell spreading increases when cells grow on more hydrophilic surfaces [14,31]. In the case of bacterial adhesion, the effects of wettability have not been so widely explored and conclu-

sions are more diverse, as they depend on many experimental factors, among which it is worth noting the high diversity in membrane properties of different bacterial strains.

Several studies using XPS analysis allowed to determine the chemical composition of the Ti6Al4V alloy surface after the Piranha etching [38–42]. This analysis confirmed that the atomic concentration of TiO_2 did not vary dramatically and the presence of suboxides such as TiO and Ti_2O_3 were observed. These observations are consistent with the model for the oxide layers proposed by McCafferty et al. [43], which is composed by three different layers, namely TiO (inner layer in contact with the metal), Ti_2O_3 (intermediate layer), and TiO_2 (outer layer). The superficial layer thus comprises a mixture of amorphous TiO_2, Al_2O_3, and small quantities of V_2O_5. This behavior is chemically plausible and can be explained by assuming that suboxides such as TiO and Ti_2O_3 are transformed into TiO_2 in the oxidative medium of Piranha solution [44,45], and by assuming that the etching solution penetrates the nanopits and reaches the underlying metal [45,46]. When the solution reaches the suboxides, they are further oxidized into TiO_2, thereby increasing the thickness of the dioxide nanoporous layer in a manner consistent with ellipsometric measurements [47,48]. This porosity increases the rate of penetration of the oxidant, and the loss of material from the surface occurs at similar rates, increasing the corrosion. In addition, the reduction in electrochemical resistance of surfaces treated with Piranha solution might have been favored by the increase in real surface area and thus, reactive surface provided by the presence of the surface nanotexture generated with this treatment. These facts, in turn, might result in decreased corrosion resistance and associated increased Ti ion release of the titanium meshes treated with Piranha solution in comparison to the HCl-treated ones. This is a potential limitation for the translation of this treatment to a clinically-used mesh and should be further studied and optimized in future work.

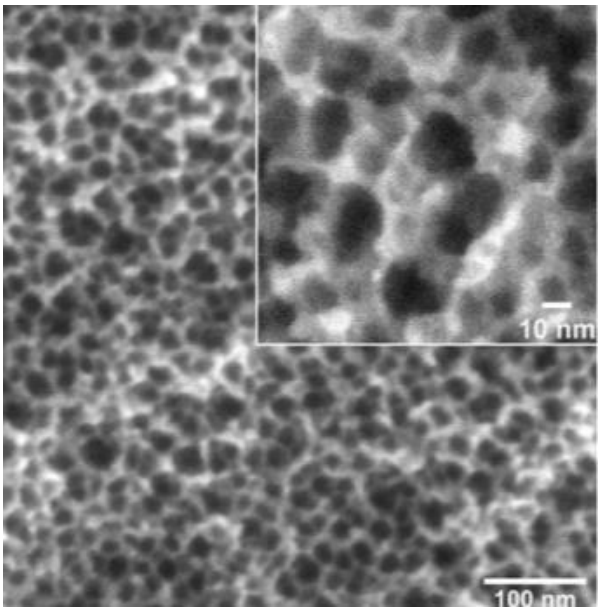

Figure 12. Nanostructure obtained in titanium meshes treated with Piranha.

We focused here on assessing the effects of the passivation treatment on bacterial adhesion, as infection is an increasing concern in the case of dental meshes. We assessed that the titanium alloy surfaces with Piranha solution prevented bacterial adhesion in a notably more effective way than non-treated and HCl-treated surfaces. It is known that bacterial adhesion is significantly hindered by surface nanotextures, typically obtained with Piranha solution treatments, as it manages to alter some structural parameters of the bacteria that determine their invasion potential [32]. Additionally, and most likely in a related way, some studies have also shown that there is a relationship between surface hydrophobicity and bacterial adhesion [35]. Hydrophobic metal surfaces favor adhesion

of hydrophobic bacteria. Both strains tested here, *S. sanguinis* and *P. aeruginosa*, are hydrophobic bacteria [36]; so, a significant decrease in bacterial adhesion could be expected on Piranha-treated surfaces that had a significantly higher surface hydrophilicity and polar character (Table 3).

The nanotexture effect is mainly caused by specific nanostructures of spike-like nanopillars, which have the capacity to mechanically destroy the murein wall of bacteria as it can be observed in titania nanotubes [49–53]. Depending on the general shape in terms of length, width and distances between these pillars, different effects such as penetration and rupture of the membrane through stretching or buckling of the bacterial wall are discussed as the actual antibacterial effect. Titania nanotubes with a diameter of 100 nm could successfully enhance gingival fibroblast proliferation and attachment while reducing the adhesion of *P. gingivalis* [54]. In this regard, there seem to be different targets in terms of how a nanostructure should be designed, and titanium biomaterials with such surfaces have not yet been introduced into the field. The antibacterial tests on Piranha-treated nanostructured substrates also confirmed a substantial reduction in bacterial growth over large areas in titanium treated with Piranha, such as *E. coli* [55] and *S. aureus* [56,57]. According to Seddiki et al., the surface features consist of 'tips' that have a sharp aspect ratio [56]. These take advantage of the fact that bacterial cells have a more rigid cell wall than eukaryotic cells. Hence, the proliferation of bacteria and such other pathogenic microorganisms onto the surface is discouraged. There is also a higher ratio of TiO_2 on the surface that contributes to the antibacterial activity [56]. Piranha-treated samples showed the highest cell viability after 24 h. This could be attributed to the change in surface morphology that allows for easy attachment of cells. However, there is no significant change in their viability even after 72 h [55]. These bacterial strains are characteristic of infections in orthopedics; in this contribution, we used aerobic and anaerobic bacteria typical in oral surgery.

It should be taken into account that this work has the limitation of ultraviolet treatment that can affect the chemical composition of the surface, but we wanted to be the closest to what actually happens. Ultraviolet light has a significant effect on the antibacterial properties of titanium surfaces. It has been reported that for titanium materials with nanostructures on the surface, when exposed to ultraviolet light for only 15 min, titanium materials show super hydrophilicity and the elimination of surface hydrocarbon pollution. Compared with those without ultraviolet light, titanium materials have lower initial bacterial adhesion and biofilm formation. The response of smooth titanium to ultraviolet light may be different from that of a titanium surface forming a nanostructure. Insufficient control of experimental variables affect the results of bacterial adhesion experiments [58].

5. Conclusions

The use of Piranha solution as an alternative passivation method for Ti6Al4V alloy for dental meshes was introduced. The Piranha treatment produced a nanotextured, hydrophilic, polar surface with anti-adhesion bacterial properties and compromised electrochemical properties. Open circuit potential and potentiodynamic tests show an increase in corrosion rate. In addition, titanium ion release is higher with Piranha treatment than HCl and control. Within the limitations of this work, we conclude that using Piranha solution could be a viable alternative method for passivating titanium dental meshes that merits further validation for its translation as a treatment applied to clinically-used meshes, taking in account the chemical degradation.

Author Contributions: Conceptualization, J.G., J.M.M., E.R. and P.V.; methodology, J.P.T., N.C. and P.V.; software, P.V.; validation, C.A. and M.P.; formal analysis, C.A.; investigation, E.R., P.V., J.G., J.P.T., N.C. and M.P.; resources, J.G.; data curation, C.A.; writing—original draft preparation, J.G.; writing—review and editing, C.A.; visualization, J.P.T. and N.C.; supervision, M.P.; project administration, E.R.; funding acquisition, J.G. All authors have read and agreed to the published version of the manuscript.

Funding: The work was supported by the Spanish Government and the Ministry of Science and Innovation of Spain by research projects RTI2018-098075-B-C21 and RTI2018-098075-B-C22 (co-funded by the European Regional Development Fund (ERDF), a way to build Europe). Authors also acknowledge Generalitat de Catalunya for funding through the 2017SGR-1165 project and the 2017SGR708 project.

Institutional Review Board Statement: Not applicable.

Informed Consent Statement: Not applicable.

Data Availability Statement: The authors can provide details of the research requesting by letter and commenting on their needs.

Acknowledgments: The authors kindly acknowledge the collaboration of Archimedes and Meritxell Molmeneu who contributed to the development of the project.

Conflicts of Interest: The authors do not have any conflict of interest.

Ethical Approval: This article does not contain any studies with human participants or animals performed by any of the authors.

References

1. Toledano-Serrabona, J.; Sanchez-Garces, M.; Sánchez-Torres, A.; Escoda, C.G. Alveolar distraction osteogenesis for dental implant treatments of the vertical bone atrophy: A systematic review. *Med. Oral. Patol. Oral. Cir. Bucal.* **2018**, *24*, 70–75. [CrossRef] [PubMed]
2. Saini, M.; Singh, Y.; Arora, P.; Arora, V.; Jain, K. Implant biomaterials: A comprehensive review. *World J. Clin. Cases* **2015**, *3*, 52–57. [CrossRef] [PubMed]
3. Lang, N.P.; Tonetti, M.S.; Suvan, J.E.; Bernard, J.P.; Botticelli, D.; Fourmousis, I.; Hallund, M.; Jung, R.; Laurell, L.; Salvi, G.E.; et al. Immediate implant placement with transmucosal healing in areas of aesthetic priority: A multicentre randomized-controlled clinical trial I. Surgical outcomes. *Clin. Oral Imp. Res.* **2007**, *18*, 188–196. [CrossRef] [PubMed]
4. Sanz-Sánchez, I.; Ortiz-Vigón, A.; Martín, I.S.; Figuero, E.; Sanz, M. Effectiveness of Lateral Bone Augmentation on the Alveolar Crest Dimension. *J. Dent. Res.* **2015**, *94*, 128–142. [CrossRef] [PubMed]
5. De Angelis, N.; Solimei, L.; Pasquale, C.; Alvito, L.; Lagazzo, A.; Barberis, F. Mechanical Properties and Corrosion Resistance of TiAl6V4 Alloy Produced with SLM Technique and Used for Customized Mesh in Bone Augmentations. *Appl. Sci.* **2021**, *11*, 5622. [CrossRef]
6. Wang, H.; Boyapati, L. "PASS" Principles for Predictable Bone Regeneration. *Implant. Dent* **2006**, *15*, 8–17. [CrossRef]
7. Levine, R.; McAllister, B. Implant Site Development Using Ti-Mesh and Cellular Allograft in the Esthetic Zone for Restorative-Driven Implant Placement: A Case Report. *Int. J. Periodontics Restor. Dent* **2016**, *36*, 373–381. [CrossRef]
8. Tan, X.; Tan, Y.J.; Chow, C.; Tor, S.B.; Yeong, W.Y. Metallic powder-bed based 3D printing of cellular scaffolds for orthopaedic implants: A state-of-the-art review on manufacturing, topological design, mechanical properties and biocompatibility. *Mater. Sci. Eng. C* **2017**, *76*, 1328–1343. [CrossRef]
9. Cruz, N.; Martins, M.I.; Santos, J.D.; Gil Mur, J.; Tondela, J.P. Surface Comparison of Three Different Commercial Custom-Made Titanium Meshes Produced by SLM for Dental Applications. *Materials* **2020**, *13*, 2177. [CrossRef]
10. Nicolas-Silvente, A.I.; Velasco-Ortega, E.; Ortiz-Garcia, I.; Monsalve-Guil, L.; Gil, J.; Jimenez-Guerra, A. Influence of the Titanium Implant Surface Treatment on the Surface Roughness and Chemical Composition. *Materials* **2020**, *13*, 314. [CrossRef]
11. Rodrigues, D.; Valderrama, P.; Wilson, T.; Palmer, K.; Thomas, A.; Sridhar, S.; Sadhwani, C. Titanium Corrosion Mechanisms in the Oral Environment: A Retrieval Study. *Materials* **2013**, *6*, 5258–5274. [CrossRef] [PubMed]
12. Godoy-Gallardo, M.; Manzanares-Céspedes, M.C.; Sevilla, P.; Nart, J.; Manzanares, N.; Manero, J.M.; Gil, F.J.; Boyd, S.K.; Rodríguez, D. Evaluation of bone loss in antibacterial coated dental implants: An experimental study in dogs. *Mater. Sci. Eng. C* **2016**, *69*, 538–545. [CrossRef] [PubMed]
13. Gil, F.J.; Rodriguez, A.; Espinar, E.; Llamas, J.M.; Padulles, E.; Juarez, A. Effect of the oral bacteria on the mechanical behavior of titanium dental implants. *Int. J. Oral. Maxillofac. Implants* **2012**, *27*, 64–68. [PubMed]
14. Mombelli, A.; van Oosten, M.A.; Schurch, E.; Land, N.P. The microbiota associated with successful or failing osseointegrated titanium implants. *Oral Microbiol. Immunol.* **1987**, *2*, 145–151. [CrossRef] [PubMed]
15. Punset, M.; Villarrasa, J.; Nart, J.; Manero, J.M.; Bosch, B.; Padrós, R.; Perez, R.A.; Gil, F.J. Citric Acid Passivation of Titanium Dental Implants for Minimizing Bacterial Colonization Impact. *Coatings* **2021**, *11*, 214. [CrossRef]
16. Duncan, W.J.; Lee, M.H.; Bae, T.S.; Lee, S.J.; Gay, J.; Loch, C. Anodisation increases integration of unloaded titanium implants in sheep mandible. *Biomed. Res. Int.* **2015**, *15*, 1–8. [CrossRef] [PubMed]
17. Kasemo, B.; Gold, J. Implant Surfaces and Interface Processes. *Adv. Dent. Res.* **1999**, *13*, 8–20. [CrossRef]
18. Variola, F.; Lauria, A.; Nanci, A.; Rosei, F. Influence of Treatment Conditions on the Chemical Oxidative Activity of H2SO4/H2O2Mixtures for Modulating the Topography of Titanium. *Adv. Eng. Mater.* **2009**, *11*, 227–234. [CrossRef]

19. Variola, F.; Francis-Zalzal, S.; Leduc, A.; Barbeau, J.; Nanci, A. Oxidative nanopatterning of titanium generates mesoporous surfaces with antimicrobial properties. *Int. J. Nanomed.* **2014**, *9*, 2319–2325. [CrossRef]
20. Brunette, D.M.; Chehroudi, B. The effects of the surface topography of micromachined titanium substrata on cell behavior in vitro and in vivo. *J. Biomech. Eng.* **1999**, *121*, 49–57. [CrossRef]
21. Jones, C.W. Applications of Hydrogen Peroxide and Derivatives. In *RSC Clean Technology, Monographs*; Royal Society of Chemistry: Cambridge, UK, 1999.
22. Bagno, A.; Di Bello, C. Surface treatments and roughness properties of Ti-based biomaterials. *J. Mater. Sci. Mater. Med.* **2004**, *15*, 939–945. [CrossRef] [PubMed]
23. Liu, Y.; Zhao, Q. Influence of surface energy of modified surfaces on bacterial adhesion. *Biophys. Chem.* **2005**, *117*, 39–46. [CrossRef] [PubMed]
24. *ASTM-E3-11*; Standard Guide for Preparation of Metallographic Specimens; ASTM International: West Conshohocken, PA, USA, 2017.
25. *ASTM G5-14e1*; Standard Reference Test Method for Making Potentiostatic and Potentiodynamic Anodic Polarization Measurements; ASTM International: West Conshohocken, PA, USA, 2014.
26. *ISO 10993-5:2009*; Biological Evaluation of Medical Devices. Part 5: Tests for In Vitro Cytotoxicity; International Organization for Standardization: Geneve, Switzerland, 2009.
27. *ASTM G-102-89*; Standard Practice for Calculation of Corrosion Rates and Related Information from Electrochemical Measurements; ASTM International: West Conshohocken, PA, USA, 2010.
28. Gil, F.J.; Rodríguez, D.; Planell, J.A.; Cortada, M.; Giner, L.; Costa, S. Galvanic corrosion behaviour of Titanium implants coupled to dental alloys. *J. Mat. Sci. Mat. Med.* **2000**, *11*, 287–293.
29. Gil, F.J.; Sánchez, L.A.; Espias, A.; Planell, J.A. In vitro corrosion behaviour and metallic ion release of different prosthodontic alloys. *Int. Dent. J.* **1999**, *49*, 347–351. [CrossRef]
30. Al-Hity, R.R.; Kappert, H.F.; Viennot, S.; Dalard, F.; Grosgogeat, B. Corrosion resistance measurements of dental alloys, are they correlated? *Dent. Mater.* **2007**, *23*, 679–687. [CrossRef] [PubMed]
31. Socransky, S.S.; Haffajee, A.D.; Cugini, M.A.; Smith, C.; Kent, R.L. Microbial complexes in subgingival plaque. *J. Clin. Periodontol.* **1998**, *25*, 134–144. [CrossRef]
32. Godoy-Gallardo, M.; Wang, Z.; Shen, Y.; Manero, J.M.; Gil, F.J.; Rodriguez, D.; Haapasalo, M. Antibacterial coatings on titanium surfaces: A comparison study between in vitro single-species and multispecies biofilm. *ACS Appl. Mater. Interfaces* **2015**, *7*, 599–601. [CrossRef]
33. Yi, J.-H.; Bernard, C.; Variola, F.; Zalzal, S.F.; Wuest, J.D.; Rosei, F.; Nanci, A. Characterization of a bioactive nanotextured surface created by controlled chemical oxidation of titanium. *Surf. Sci.* **2006**, *600*, 4613–4621. [CrossRef]
34. Castner, D.G.; Ratner, B.D. Biomedical surface science: Foundations to frontiers. *Surf. Sci.* **2002**, *500*, 28–60. [CrossRef]
35. Wheelis, S.E.; Gindri, I.M.; Valderrama, P.; Wilson, T.G., Jr.; Huang, J.; Rodrigues, D.C. Effects of decontamination solutions on the surface of titanium: Investigation of surface morphology, composition, and roughness. *Clin. Oral Implants Res.* **2015**, *27*, 329–340. [CrossRef]
36. Heitz-Mayfield, L.J.; Lang, N.P. Comparative biology of chronic and aggressive periodontitis vs. peri-implantitis. *Periodontol 2000* **2010**, *531*, 67. [CrossRef] [PubMed]
37. Michiardi, A.; Aparicio, C.; Ratner, B.D.; Planell, J.A.; Gil, J. The influence of surface energy on competitive protein adsorption on oxidized NiTi surfaces. *Biomaterials* **2007**, *28*, 586–594. [CrossRef] [PubMed]
38. Variola, F.; Yi, J.H.; Richert, L.; Wuest, J.D.; Rosei, F.; Nanci, A. Tailoring the surface properties of Ti6Al4V by controlled chemical oxidation. *Biomaterials* **2008**, *29*, 1285–1298. [CrossRef]
39. Muhonen, V.; Heikkinen, R.; Danilov, A.; Jamsa, T.; Tuukkanen, J. The effects of oxide thickness on osteoblast attachment and survival on NiTi alloy. *J. Mater. Sci. Mater. Med.* **2007**, *18*, 959–967. [CrossRef] [PubMed]
40. Amor, S.B.; Baud, G.; Besse, J.P.; Jacquet, M. Structural and optical properties of sputtered titania films. *Mater. Sci. Eng. B* **1997**, *47*, 110–118. [CrossRef]
41. Velten, D.; Biehl, V.; Aubertin, F.; Valeske, B.; Possart, W.; Breme, J. Preparation of TiO_2 layers on cp-Ti and Ti_6Al_4V by thermal and anodic oxidation and by sol-gel coating techniques and their characterization. *J. Biomed. Mater. Res.* **2002**, *59*, 18–28. [CrossRef]
42. Amor, S.B.; Guedri, L.; Baud, G.; Jacquet, M.; Ghedira, M. Influence of the temperature on the properties of sputtered titanium oxide films. *Mater. Chem. Phys.* **2002**, *77*, 903–911. [CrossRef]
43. McCafferty, E.; Wightman, J.P. An X-ray photoelectron spectroscopy sputter profile study of the native air-formed oxide film on titanium. *Appl. Surf. Sci.* **1999**, *143*, 92–100. [CrossRef]
44. Arys, A.; Philippart, C.; Dourov, N.; He, Y.; Le, Q.T.; Pireaux, J.J. Analysis of titanium dental implants after failure of osseointegration: Combined histological, electron microscopy, and X-ray photoelectron spectroscopy approach. *J. Biomed. Mater. Res.* **1998**, *43*, 300–312. [CrossRef]
45. Lee, T.M.; Chang, E.; Yang, C.Y. Surface characteristics of Ti6Al4V alloy: Effect of materials, passivation and autoclaving. *J. Mater. Sci. Mater. Med.* **1998**, *9*, 439–448. [CrossRef]
46. Pouilleau, J.; Devilliers, D.; Garrido, F.; Durand-Vidal, S.; Mahe, E. Structure and composition of passive titanium oxide films. *Mater. Sci. Eng. B* **1997**, *47*, 235–243. [CrossRef]

47. Lisowski, W.; van den Berg, A.H.J.; Smithers, M. Characterization of titanium hydride film after long-term air interaction: SEM, ARXPS and AES depth profile studies. *Surf. Interface Anal.* **1998**, *26*, 213–219. [CrossRef]
48. Pegueroles, M.; Aparicio, C.; Bosio, M.; Engel, E.; Gil, F.J.; Planell, J.A.; Altankov, G. Spatial organization of osteoblast fibronectin matrix on titanium surfaces: Effects of roughness, chemical heterogeneity and surface energy. *Acta Biomater.* **2010**, *6*, 291–301. [CrossRef] [PubMed]
49. Mukaddam, K.; Astasov-Frauenhoffer, M.; Fasler-Kan, E.; Marot, L.; Kisiel, M.; Meyer, E.; Köser, J.; Waser, M.; Bornstein, M.M.; Kühl, S. Effect of a Nanostructured Titanium Surface on Gingival Cell Adhesion, Viability and Properties against *P. gingivalis*. *Materials* **2021**, *14*, 7686. [CrossRef] [PubMed]
50. Ivanova, E.P.; Hasan, J.; Webb, H.K.; Truong, V.K.; Watson, G.S.; Watson, J.A.; Baulin, V.A.; Pogodin, S.; Wang, J.Y.; Tobin, M.J.; et al. Natural Bactericidal Surfaces: Mechanical Rupture of Pseudomonas Aeruginosa Cells by Cicada Wings. *Small* **2012**, *8*, 2489–2494. [CrossRef] [PubMed]
51. Ivanova, E.P.; Hasan, J.; Webb, H.K.; Gervinskas, G.; Juodkazis, S.; Truong, V.K.; Wu, A.H.F.; Lamb, R.N.; Baulin, V.A.; Watson, G.S.; et al. Bactericidal Activity of Black Silicon. *Nat. Commun.* **2013**, *4*, 2838. [CrossRef] [PubMed]
52. Serrano, C.; García-Fernández, L.; Fernández-Blázquez, J.P.; Barbeck, M.; Ghanaati, S.; Unger, R.; Kirkpatrick, J.; Arzt, E.; Funk, L.; Turón, P.; et al. Nanostructured Medical Sutures with Antibacterial Properties. *Biomaterials* **2015**, *52*, 291–300. [CrossRef]
53. Jenkins, J.; Mantell, J.; Neal, C.; Gholinia, A.; Verkade, P.; Nobbs, A.H.; Su, B. Antibacterial Effects of Nanopillar Surfaces Are Mediated by Cell Impedance, Penetration and Induction of Oxidative Stress. *Nat. Commun.* **2020**, *11*, 1626. [CrossRef]
54. Xu, Z.; He, Y.; Zeng, X.; Zeng, X.; Huang, J.; Lin, X.; Chen, J. Enhanced Human Gingival Fibroblast Response and Reduced Porphyromonas Gingivalis Adhesion with Titania Nanotubes. *Biomed. Res. Int.* **2020**, *2020*, 5651780. [CrossRef]
55. Kiran, A.S.; Kumar, T.S.; Perumal, G.; Sanghavi, R.; Doble, M.; Ramakrishna, S. Dual nanofibrous bioactive coating and antimicrobial surface treatment for infection resistant titanium implants. *Progress in Organic Coatings* **2018**, *121*, 112–119. [CrossRef]
56. Seddiki, O.; Harnagea, C.; Levesque, L.; Mantovani, D.; Rosei, F. Evidence of antibacterial activity on titaniumsurfaces through nanotextures. *Appl. Surf. Sci.* **2014**, *308*, 275–284. [CrossRef]
57. Skindersoe, M.E.; Krogfelt, K.A.; Blom, A.; Jiang, G.; Prestwich, G.D.; Mansell, J.P. Dual Action of Lysophosphatidate-Functionalised Titanium:Interactions with Human (MG63) Osteoblasts and Methicillin Resistant Staphylococcus aureus. *PLoS ONE* **2015**, *10*, e0143509. [CrossRef] [PubMed]
58. Vermeulen, N.; Werden, J.; Keeler, W.J.; Nandakumar, K.; Leung, K.T. The Bactericidal Effect of Ultraviolet and Visible Light on Escherichia Coli. *Biotechnol. Bioeng.* **2008**, *99*, 550–556. [CrossRef] [PubMed]